Regulation of eIF4F Translation Initiation Complex by the Peptidyl Prolyl Isomerase FKBP7 in Taxane-resistant Prostate Cancer

Marine F Garrido, Nicolas J.-P. Martin, Matthieu Bertrand, Catherine Gaudin, Frédéric Commo, Nassif El Kalaany, Nader Al Nakouzi, Ladan Fazli, Elaine del Nery, Jacques Camonis, et al.

Author Manuscript Published OnlineFirst on October 15, 2018; DOI: 10.1158/1078-0432.CCR-18-0704
Author manuscripts have been peer reviewed and accepted for publication but have not yet been edited.

Regulation of eIF4F translation initiation complex by the peptidyl prolyl isomerase FKBP7 in taxane-resistant prostate cancer

Marine F. Garrido[1,2,3], Nicolas J-P. Martin[1,2,3], Matthieu Bertrand[1,2,3], Catherine Gaudin[1,2,3], Frédéric Commo[1,2,3], Nassif El Kalaany[1,2,3],Nader Al Nakouzi[4], Ladan Fazli[4], Elaine Del Nery[5,6], Jacques Camonis[5,6,7], Franck Perez[5,6,8], Stéphanie Lerondel[9], Alain Le Pape[9], Daniel Compagno[10],Martin Gleave[4], Yohann Loriot[1,2,3], Laurent Désaubry[11], Stephan Vagner[5,12], Karim Fizazi[1,2,3], Anne Chauchereau[1,2,3]

[1]Prostate Cancer Group, INSERM UMR981, Villejuif, F-94805, France
[2]Univ Paris-Sud, UMR981, Villejuif, France
[3]Gustave Roussy, Villejuif, France
[4]Vancouver Prostate Centre and Department of Urologic Sciences, University of British Columbia, Canada
[5]Institut Curie, PSL Research University
[6]Biophenics High-Content Screening Laboratory, Cell and Tissue Imaging Facility (PICT-IBiSA), 75005 Paris, France
[7]INSERM, U830, F-75005, Paris, France.
[8]CNRS, UMR144, F-75005, Paris, France
[9]PHENOMIN-TAAM, CIPA, CNRS UPS44, Orléans, France
[10]Molecular and Functional Glyco-Oncology Lab, IQUIBICEN-CONICET, Facultad de Ciencias Exactas y Naturales-Universidad de Buenos Aires, CABA, Argentina.
[11]CNRS UMR7200, Strasbourg University, Illkirch, France
[12]CNRS, UMR3348, F-91405, Orsay, France

Running title: FKBP7, a new target in taxane-resistant prostate cancer

Key words: Prostate cancer; Taxane resistance; Chemoresistance; Molecular chaperone; FKBP7; eIF4F

Corresponding author:
Anne Chauchereau, Prostate Cancer Group, INSERM UMR981, 94805 Villejuif, France
Tel: +33142116607 E-mail: anne.chauchereau@gustaveroussy.fr

The authors declare no potential conflicts of interest

STATEMENT OF TRANSLATIONAL RELEVANCE

Taxane-based therapies are currently used for the clinical treatment of prostate cancer, but treatment usually fails after time as resistance emerges requiring new therapeutic strategies to overcome taxane-resistance and improve outcomes for men with prostate cancer.

Our study reveals the critical role played by FKBP7, a still uncharacterized chaperon protein as a novel mediator of taxane resistance in prostate cancer. The finding that FKBP7 interacts and regulates the level of the translation initiation factor eIF4G will allow targeting FKBP7 or the eIF4G-containing eIF4F complex, as a novel therapeutic strategy in chemoresistant prostate cancer.

ABSTRACT

PURPOSE: Targeted therapies that use the signaling pathways involved in prostate cancer are required to overcome chemoresistance and improve treatment outcomes for men. Molecular chaperones play a key role in the regulation of protein homeostasis and are potential targets for overcoming chemoresistance.

EXPERIMENTAL DESIGN: We established four chemoresistant prostate cancer cell lines and used image-based high-content siRNA functional screening, based on gene-expression signature, to explore mechanisms of chemoresistance and identify new potential targets with potential roles in taxane resistance. The functional role of a new target was assessed by *in vitro* and *in vivo* silencing, and mass spectrometry analysis was used to identify its downstream effectors.

RESULTS: We identified FKBP7, a prolyl-peptidyl isomerase overexpressed in docetaxel-resistant and in cabazitaxel-resistant prostate cancer cells. This is the first study to characterize the function of human FKBP7 and explore its role in cancer. We discovered that FKBP7 was upregulated in human prostate cancers and its expression correlated with the recurrence observed in patients receiving docetaxel. *FKBP7* silencing showed that FKBP7 is required to maintain the growth of chemoresistant cell lines and chemoresistant tumors in mice. Mass spectrometry analysis revealed that FKBP7 interacts with eIF4G, a component of the eIF4F translation initiation complex, to mediate the survival of chemoresistant cells. Using small molecule inhibitors of eIF4A, the RNA helicase component of eIF4F, we were able to kill docetaxel and cabazitaxel-resistant cells.

CONCLUSION: Targeting FKBP7 or the eIF4G-containing eIF4F translation initiation complex could be novel therapeutic strategies to eradicate taxane-resistant prostate cancer cells.

INTRODUCTION

Molecular chaperones are upregulated and associated with resistance to treatment in castration-resistant prostate cancer (CRPC) (1,2), an advanced form of prostate cancer that develops when the disease progresses after initial treatment with surgery and/or medical castration using androgen deprivation therapy (ADT). Docetaxel and cabazitaxel are two taxane chemotherapies that are approved for treatment of metastatic CRPC (3). Recent studies have reported benefits when docetaxel was combined with ADT during the hormone-sensitive stage of the disease (3,4). Unfortunately, approximately 50% of patients do not respond to docetaxel. Taxane resistance mechanisms include decreased cellular drug accumulation due to membrane-bound efflux protein overexpression, tubulin isotope overexpression, and defects in apoptosis (5,6). Many of these pathways involve molecular chaperones, but strategies for targeting them have encountered only limited efficacy. New therapeutic strategies are needed to overcome taxane-resistance and improve outcomes for men with prostate cancer.

Several molecular chaperones, including heat-shock proteins Hsp27 and Hsp90, clusterin (CLU) and FKB506-binding proteins (FKBPs), are involved in protein folding, cellular signaling, apoptosis and transcription, and are potential targets for cancer treatment (7,8). FKBP12 (*FKBP1A*) was the first enzyme shown to bind FK506, a natural immunosuppressant, and rapamycin, a macrolide indicated in organ rejection prophylaxis after renal transplantation (9). FKBP12-rapamycin complex associates with the major downstream Akt mammalian target of rapamycin mTOR-kinase (mammalian target of rapamycin kinase) and has immunosuppressive and antiproliferative properties. Larger FKBPs, such as FKBP52 (*FKBP4*) and FKBP51 (*FKBP5*), have also been shown to form rapamycin-induced ternary complexes that inhibit mTOR-kinase activity. FKBP51 and FKBP52 regulate the microtubule-associated protein, tau, and thus affect microtubule stability (10). FKBP7, a molecular chaperone cloned from mouse heart (11), is located in the endoplasmic reticulum and has been shown to

suppress the ATPase activity of mouse ER chaperone HSPA5/GRP78/Bip by its prolyl-peptidyl isomerase activity (11,12).

Here, we established four chemoresistant prostate cancer cell lines to explore mechanisms of taxane resistance, and investigated the FKBP7 signaling pathway and its potential role in taxane resistance in human prostate cancer patients.

METHODS

Cell lines

Parental and taxane-resistant IGR-CaP1, PC3, LNCaP and 22RV1 human PCa cell lines were maintained in RPMI1640 medium with 10% fetal bovine serum. Pooled taxane-resistant populationss were obtained by exposing cells to docetaxel (Sanofi-Aventis) or cabazitaxel (Selleckchem) in a dose-escalation manner as described for IGR-CaP1 (13). Resistant cell lines were treated monthly with the maximum dose of docetaxel or cabazitaxel to maintain the resistant phenotype. Other cell lines are detailed in Supplementary Information.

Microarray

Gene expression was profiled using a 4×44K human whole genome (G4112F) expression array (Agilent Technologies) with dual-color dye-swap competitive hybridization. Total RNA from untreated parental IGR-CaP1 cells was the RNA reference. Total RNA from IGR-CaP1 cells resistant to 5, 12, 25 50, 100 and 200nM of docetaxel were used as samples (two replicates/sample). Image (Feature Extraction software: Agilent Technologies) and gene expression (Bioconductor) analyses was performed.

For resistant cell lines, Log10 ratios were computed against the relevant sensitive cell line. To select relevant genes we combined three strategies. Genes permanently over/under-expressed in all resistant cell lines were tested using multiple t-tests with bootstrap resampling-based analysis

(10,000 samples with replacement). Resulting *p*-values were adjusted using the Benjamini-Hochberg correction method (14) (adjusted *p*-values ≤0.05 considered as significant). Genes with monotonic increasing/decreasing expression over increasing doses were tested using 5-parameter logistic regression (14). The decision rule combined an absolute fold change of ≥2 between the upper and lower asymptotes, and an adjusted *p*-value ≤1e-3, representing correlation quality between the fitted and observed values. Supplementary, potentially informative genes were selected using an information criterion method with reversed principal component analysis (probes considered as observations). An information criterion per gene was computed to quantify its ability to separate samples and 998 genes potentially implicated in docetaxel resistance were identified (593 upregulated and 407 down-regulated). Image-based high-content siRNA screening, data analysis and hit calling are detailed in Supplementary information.

Tissue microarray staining and analysis

Prostate tissue samples used for the tissue microarray (TMA) were obtained from the Vancouver Prostate Centre Tissue Bank. This study followed the ethical guidelines stated in the Declaration of Helsinki, specimens were obtained from patients with their informed written consent form following a protocol approved by the Institutional Review Board of the University of British Columbia (UBC). The H&E slides were reviewed and the desired areas were identified.

Eight TMAs were constructed (Beecher Instruments) by punching duplicate 1mm cores per sample. All specimens (n=381) were obtained through radical prostatectomy, except CRPC samples obtained via transurethral resection of the prostate.

Two TMAs were constructed from 90 patients who had received docetaxel after radical prostatectomy. Analysis was performed on 69 selected cancer patients with good core integrity. Immunostaining was performed using an automatized technique (Biotin-Streptavidin system and solvent-resistant DAB Map kit) with a Discover XT™ autostainer (Ventana Medical System). Slides were digitized with the SL801 autoloader and Leica SCN400 scanning system (Leica Microsystems; ×20 magnification). Clearly positive/negative and mixed positive/negative cores were identified.

FKBP7 staining was analyzed (0: no staining; 1: faint or focal stain; 2 and 3: convincingly intense stain in most cells).

SiRNA transfection

Cell transfection was performed for siRNA sequences (see Supplementary Information). Cells were plated in 96-well plates with 20nM siRNA for reverse transfection. Transfection efficiency was checked by western-blot.

Western blot

Immunoblots were prepared using whole cell lysate with RIPA buffer, protease inhibitors (Roche) and phosphatase inhibitors (Sigma-Aldrich), then analyzed using an enhanced chemoluminescence-based detection kit (Pierce). See Supplementary Information for Antibody sources.

ShRNA knockdown in docetaxel-resistant (Dtx-R) mouse model

Animal experiments were approved by the local ethics committee (CEEA IRCIV/IGR no. 1226.01, registered with the French Ministry of Research) and performed in compliance with EU Directive 63/2010. IGR Animal Resources holds a Department of Health and Human Services Animal Welfare Insurance (no. A5660-01) and complies with the Guide for the Care and Use of Laboratory Animals.

The Dtx-R mouse model (Supplementary Fig. S4A) was established in nude mice (see Supplementary Information). Two shRNAs targeting FKBP7 (shFK-1 and shFK-2) were engineered and packaged using the GIPZ lentivirus delivery system (see Supplementary information for details). Two 10^6 IGR-Rvivo cells transduced with sh-ctrl, skFK-1 or shFK-2 (in 100µl PBS with 50% Matrigel) were injected subcutaneously in NOD Scid gamma mice purchased from the IGR Animal Resources. Tumor growth was monitored for 50-70 days. When tumors reached an average volume of 450-500mm^3, mice were injected intraperitoneally, three times with docetaxel at 30mg/kg or vehicle, once every 3 weeks.

Mass spectrometry analysis

IGR-CaP1-Dtx-R and RPE-1 cells were grown in 4 T150 flasks and harvested at ~80% confluency. Cells were lysed and ~10mg proteins were extracted twice for 30 minutes in buffer (120mM NaCl, 20mM

Hepes, 1mM EDTA, 5% glycerol, 0.5% NP40 and protease inhibitor). Pooled supernatants were incubated overnight with 6µg of either control IgG or FKBP7 antibodies, and 50µl of magnetic beads (Dynabeads® Protein A, Thermo Fisher Scientific). After 4 washes, protein complexes were eluted twice in LDS buffer (Thermo Fisher Scientific) and loaded onto 10% Bis-Tris protein gel. After 5 min of migration, the band containing the proteins was excised and processed [standard protocol (15)]. Peptide mixtures were analyzed on EASY 1000nLC + Q-EXACTIVE (Thermo Fisher Scientific), using an EASY-Spray nanocolumn (ES800 15cm 75um), 300 nl/min flow and 2h gradient of acetonitrile + 0.1% formic acid (5% starting and 35% final acetonitrile concentrations). Mass resolution for the full scan was set at 70,000 at 400 m/Z. The 10 most intense precursor ions from a survey scan were selected for MS/MS fragmentation using high-energy collision dissociation fragmentation with 27% normalized collision energy (detected at mass resolution 17,500 at 400 m/z). Dynamic exclusion was set for 30 seconds with a 10 ppm mass window. Each sample was analyzed in triplicate. The acquired data were analyzed with Proteome Discoverer software using a Mascot search engine (Proteome ID UP000005640; 20253 sequences). MS/MS spectra were searched with a precursor mass tolerance of 10 ppm and fragment mass tolerance of 0.05 Da. Trypsin was specified as protease with a maximum of two missed cleavages allowed. The minimum peptide length was specified as 6 amino acids. Data were searched against a decoy database, and the false discovery rate was set at 1% of the peptide level. FKBP7 interactors were selected when proteins (compared to IgG control) were only identified in the FKBP7 immunoprecipitation or were enriched at least 3-fold in the specific immunoprecipitation. Specific protein interactors were processed [Ingenuity Pathway Analysis® (IPA)].

SILAC (stable isotope labeling by amino acids in cell culture) analysis

IGR-CaP1-Dtx-R or RPE-1 cells were adapted, respectively, to RPMI or DMEM:F12 SILAC media containing either 12C6, 14N4 L-Arginine-HCl + 12C6 L-Lysine-2HCl (light media) or 13C6, 15N4 L-Arginine-HCl + 13C6 L-Lysine-2HCl (heavy media) (Thermo Fisher Scientific) for a minimum of 5 cell doublings. Cells grown in heavy media were transfected with control siNT and cells cultured in light

media were transfected with si-FKBP7-2. Equal amounts of cells were mixed and lysed in LDS sample buffer and reducing agent (Thermo Fisher Scientific). Samples were loaded onto NuPage 10% Bis-Tris protein gel and proteins were allowed to enter the gel (with application of 150 Volts) for only 5 minutes, then the protein-containing band was excised and processed [standard protocol (16)]. Analysis of the obtained peptide mixtures was performed as described above, except the H/L ratio per peptide, which was calculated by the quantitation node. The average light to heavy ratio was calculated per identified protein and the lists of proteins in IGR-CaP1-Dtx-R and RPE-1 were processed through IPA.

Proximity ligation assay

FKBP7-eIF4G and eiF4E-eiF4G interactions were detected by *in situ* proximity ligation assay (PLA) (Duolink, Sigma-Aldrich). Cells were fixed with paraformaldehyde, permeabilized and the PLA protocol was performed (Olink Bioscience). After blocking, primary antibodies were incubated for 1h at 37°C. PLA® probe secondary antibodies were incubated for 1h at 37°C. After ligation and DNA amplification, amplicons were detected using far red fluorescence, nuclei were stained with DAPI and slides were mounted with Olink Mounting Medium. Images were acquired with a Virtual Slides VS120-SL microscope [Olympus, Tokyo, Japan; magnification 20X, air objective (0.75 NA), 10-ms exposure for the DAPI channel and 300-ms exposure for the Cy5 channel; 1pixel=0.32µm] and the number of PLA signals/cell was counted using Image Analysis toolbox in Matlab (2011a).

Statistical Analysis

For the TMA, FKBP7 staining was analyzed with the Chi-square test and the recurrence % was calculated with a Fisher test. Kaplan–Meier curve statistical significance *p*-values were calculated using the Cox proportional hazard model. Cell proliferation curves and tumor growth curves were analyzed by a two-way ANOVA with Bonferroni post-tests. The significance of the mRNA coding level for eiF4G when FKBP is silenced was set with a Student t-test. The significance of eIF4G-FKBP7 and eIF4E-eIF4G interactions was tested with the linear model or Wilcoxon rank test.

150

151

152 **Accession number**

153 Microarray experiments were submitted to the Array Express data base (EBI, UK)

154 (www.ebi.ac.uk/arrayexpress/), accession number E-MTAB-4869. MS data were deposited in PRIDE

155 (www.ebi.ac.uk/pride/).

156

RESULTS

FKBP7 is upregulated during the progression of chemoresistant CRPC

To decipher the mechanisms of taxane resistance in prostate cancer, we developed a series of 4 isogenic parental, docetaxel-resistant (Dtx-R), and cabazitaxel-resistant (Cbx-R) cell lines representative of the different types of epithelial prostate cancer cells (Supplementary Fig. S1). By comparing the gene expression profiles of parental and Dtx-R cells (13,17), we generated a signature of 998 highly differentially-expressed genes potentially correlating with chemoresistance (Supplementary Table S1A-B). Following image-based high-content screening in which the 593 upregulated genes were independently targeted with 4 siRNAs, we identified 34 genes required for cell survival of IGR-CaP1-Dtx-R cells, for which at least 2 siRNAs showed robust Z-scores >2 for G0 cell-cycle arrest phenotype modification and cell proliferation (Supplementary Table S2A-B). We focused on chaperone proteins responsive to stress. In particular, as already reported (18,19), the ER chaperone protein HSPA5 (GRP78/BiP) was sorted as a candidate involved in chemoresistance in our model. Considering that HSPA5 has been shown to interact with FKBP7 chaperone in a mouse model (12), we focused on the potential role of the uncharacterized FKBP7 human protein, one of the hits during screening, in the mechanism of taxane resistance in prostate cancer.

FKBP7 protein levels were higher in the four parental prostate cancer cell lines compared to RWPE-1 non-cancerous prostate cells (Fig. 1A), and in all Dtx-R and Cbx-R cells compared to their respective parental cells, with an 8 fold-change in taxane-resistant IGR-CaP1 cells. Increased FKBP7 protein levels were related to gene expression upregulation, as we found more FKBP7 mRNA in the taxane-resistant cells than in parental cells (Supplementary Fig. S2A). An increase in FKBP7 expression was an early response of cells observed after 48h-72h of treatment with microtubule-targeting agents such as taxanes and nocodazole (Fig. 1B and Supplementary Fig. S2B). In contrast, FKBP7 was not overexpressed in enzalutamide-resistant 49F and 42D cells generated from an *in vivo* LNCaP model (20,21) compared to the enzalutamide-sensitive V16D cells (Fig. 1C).

To investigate the physiological relevance of FKBP7 expression in prostate cancer, we determined FKBP7 expression by immunohistochemistry using tissue microarrays containing 381 prostate cancer and benign tissues obtained from radical prostatectomy or transurethral resection (Supplementary Table S3). Consistent with observations in non-cancerous RWPE-1 cells *versus* CaP cell lines in Fig1A, higher FKBP7 expression was seen in prostate cancers than in benign tissues (Fig. 1D). Quantification of staining intensities showed that FKBP7 levels were significantly higher in prostate cancers than in benign tissues (Fig. 1D).

We evaluated FKBP7 expression using TMAs comprising a subset of 69 prostate cancers from patients who had received docetaxel as neoadjuvant therapy. High FKBP7 levels correlated significantly with recurrence % in patients (post-surgical prostate cancer recurrence, metastasis or death); 79% of patients with high FKBP7 levels developed recurrence compared to 42% of patients with low FKBP7 (Fig. 1E). High levels of FKBP7 were significantly associated with a shorter time to recurrence in patients (p=0.004; hazard ratio for low FKBP7: 0.3846) (Fig. 1F). Levels of FKBP7 during progression to lethal prostate cancer did not correspond to gene mutations in published data from whole exome sequencing in docetaxel-treated CRPC patients (22). These results show strong correlations between FKBP7 levels and resistance to cytotoxic treatment in prostate cancer.

SiRNA-mediated FKBP7 knock-down blocks chemoresistant cell growth and increases apoptosis in taxane-treated resistant cells

To determine whether FKBP7 could be a therapeutic target in chemoresistant prostate cancer, we used 2 siRNA sequences targeting FKBP7 to knock-down FKBP7 expression in chemoresistant cells. A statistically significant decrease in chemoresistant cell growth was observed after FKBP7 silencing (Fig. 2A). Except for 22RV1 cells, a similar effect was observed in the parental cells (Supplementary Fig. S3A). FKBP7 silencing induced slight apoptosis of chemoresistant cells, and PARP cleavage was further increased after treatment with docetaxel and cabazitaxel (Fig. 2B). This chemosensitization effect was not observed by measuring cell growth over the same time-course (Supplementary Fig. S3B). Conversely, FKBP7 overexpression is not sufficient to render prostate cancer cells more

resistant to taxanes as shown in parental IGR-CaP1 and 22R1 cells transduced with lentivirus expressing FKBP7 (Supplementary Fig. S3C). These results show that FKBP7 is not a primary event of the acquisition of the resistant state but show the importance of FKBP7 signaling in maintaining the chemoresistance state.

FKBP7 silencing reduces tumor growth in docetaxel-resistant mice

The IGR-CaP1 cell line was used to generate a chemoresistant mCRPC mouse model. Various clones of IGR-CaP1 resistant to docetaxel were injected subcutaneously into nude mice. The 25nM-resistant emerging tumor was maintained *in vivo* for 5 successive passages to increase the tumorigenicity (Supplementary Fig. S4A). These IGR-CaP1-Rvivo tumors did not respond to 3 successive injections of 30mg/kg docetaxel, therefore constituting a new Dtx-R mouse model, whereas the parental IGR-CaP1 mouse model responded to docetaxel (Fig. 3A). A new IGR-CaP1-Rvivo cell line generated from the IGR-CaP1-Rvivo tumors showed chemoresistant characteristics (with IC_{50}=207nM towards docetaxel) (Fig. 3B). In addition, and in agreement with results obtained *in vitro* and in human samples, the resistant IGR-CaP1-Rvivo cell line showed high levels of FKBP7 (Fig. 3B). Thus, to check whether FKBP7 could be a therapeutic target in Dtx-R mice, we established two IGR-CaP1-Rvivo cell lines in which FKBP7 was stably silenced with two different shRNAs. A substantial reduction of FKBP7 level was achieved in cells that were stably expressing shRNAs targeting FKBP7 (shFK-a and shFK-b), compared to control shRNA-expressing cells (Fig. 3C). ShRNA-transduced cell lines were subsequently injected subcutaneously in immunodeficient mice. In the absence of docetaxel, significantly reduced tumor growth was observed after FKBP7 depletion (68% and 47% inhibition of tumor growth in shFK-a- and -b-transduced cells, respectively), *versus* control shRNA-transduced cell line (Fig. 3C). This effect was more pronounced in the xenograft from the shFK-a cells showing a high reduction of FKBP7 to a level similar to that observed in the parental sensitive cells, suggesting that FKBP7 sustains the growth of chemoresistant tumors. Treatment of mice with docetaxel when tumors reached 450-500mm^3 strongly abrogated the growth of shFK-a-transduced tumors, while it slightly decreased the growth of control shRNA-transduced tumors (Fig. 3C). Consistently, *in vitro*

proliferation data showed that shFK-a-transduced cells are more sensitive to higher dose of taxanes (Supplementary Fig. S4B). Thus these results demonstrate that *in vitro* and *in vivo* FKBP7 silencing inhibits cell proliferation and sensitizes chemoresistant cells to taxanes, and that FKBP7 can be a relevant therapeutic target to overcome chemoresistance in prostate cancer.

FKBP7 silencing does not affect cell growth in non-tumorous cells

We determined the levels of FKBP7 in non-cancerous human cell lines of different origins (fibroblastic, myoblastic, epithelial and endothelial cells). These non-cancerous cells showed a high level of FKBP7, which was similar (in RPE-1) or even higher than that observed in IGR-CaP1-Dtx-R cells (Supplementary Fig. S5A), but in contrast to the results obtained in chemoresistant cells, we observed no effect of FKBP7 inhibition on cell growth or viability (Supplementary Fig. S5B), suggesting that FKBP7 could have different functions in cancerous and non-cancerous cells.

FKBP7 interacts with eukaryotic translation initiation factors to regulate protein translation

To identify molecular pathways in which FKBP7 functions in non-cancerous and chemoresistant cells, we performed qualitative and quantitative mass spectrometry analyses. The protein interactome of FKBP7 was identified by immunoprecipitating endogenous FKBP7 with two antibodies in non-cancerous RPE-1 and Dtx-R IGR-CaP1 cell lines (Supplementary Table S4A-B). Protein network analysis through IPA indicated that in both cell lines, FKBP7 protein interactors were mainly distributed in the same three intracellular pathways associated with protein translation. Specifically, eIF2, eIF4 and mTOR signaling were the most represented pathways in the signatures (Fig. 4A), and many eukaryotic translation initiation factors were represented. To elucidate the molecular mechanisms by which FKBP7 depletion exerts its cytotoxic effects in chemoresistant cells only, we used SILAC in FKBP7-silenced RPE-1 and IGR-CaP1-Dtx-R cells and in cells transfected with control siRNA, and we obtained lists of 910 and 1223 differentially expressed proteins in RPE-1 and in IGR-CaP1-Dtx-R cells, respectively (Supplementary Table S5A-B). Consistently with previous results, IPA analysis showed that the major pathways affected by FKBP7-silencing were the same three pathways implicated in protein translation control; based on calculated Z-score, these pathways were

downregulated in IGR-CaP1-Dtx-R cells, but mainly upregulated in non-cancerous RPE-1 cells (Fig. 4B-C). All three individual components of the eIF4F cap-dependent mRNA translation complex (eIF4E, eIF4A and eIF4G) were identified as protein partners of FKBP7 in resistant and RPE-1 cells. Co-immunoprecipitation experiments confirmed the interaction of FKBP7 with eIF4G (Fig. 4D and Supplementary Fig. S6A), but interaction of FKBP7 with eIF4A was not detectable (Supplementary Fig. S6A).

FKBP7 regulates the level of eIF4F complexes

EIF4F is an interesting target, known to be involved in resistance mechanisms to many cancer therapies (23–26). We focused on eIF4G, the most downregulated eukaryotic translation factor in IGR-CaP1-Dtx-R cells, but not in RPE-1 cells. FKBP7-silencing led to decreased eIF4G in IGR-CaP1-Dtx-R cells, but to increased eIF4G in corresponding non-cancerous RPE-1 cells (Fig. 5A). The level of eIF4G was also lower in other chemoresistant cellular models (Fig. 5B) and in parental cells (Supplementary Fig. S6B). In contrast, protein levels of eIF4A and eIF4E remained unchanged after FKBP7 silencing (Fig. 5A).

To understand how FKBP7 silencing decreased eIF4G level, we analyzed the effect of FKBP7 depletion on eIF4G gene expression. Efficient FKBP7 silencing did not affect eIF4G mRNA levels in FKBP7-silenced chemoresistant IGR-CaP1 and 22RV1 cells (Supplementary Fig. S6C), so our results showed that while eIF4G is still transcribed, its protein level decreases when FKBP7 is silenced, thus leading to the hypothesis that FKBP7 regulates eIF4G expression at mRNA translation or protein stability levels. Treatment with the translation inhibitor cycloheximide combined with FKBP7 silencing showed that although the steady-state level of eIF4G was decreased upon FKBP7 silencing, the amount of eIF4G in control cells decreased over time whereas it was stable in FKBP7-depleted cells supporting the hypothesis that FKBP7 regulates eIF4G expression at the protein level (Fig. 5C). However, we cannot exclude the possibility of an increase in eIF4G mRNA translation to compensate the protein loss observed when FKBP7 was silenced. We therefore investigated the ability of FKBP7

to interact with eIF4G by performing PLA, allowing the interaction to be quantitatively visualized as fluorescent dots. Our results revealed an interaction between FKBP7 and eIF4G in Dtx-R-IGR-CaP1 and Dtx-R-22RV1 cells (Fig. 5E). This interaction was largely affected in FKBP7- and eIF4G-depleted cells, as shown by the lower numbers of dots/cell (43% and 80% reduction in IGR-CaP1-Dtx-R cells, 93% and 86% in 22RV1-Dtx-R cells, for FKBP7- and eIF4G-silencing respectively) (Fig. 5E); the silencing of eIF4G was very efficient (Fig. 5D) and the specificity of the FKBP7-eIF4G interaction was validated (Supplementary Fig. S6D).

As FKBP7 interacts with eIF4G and modulates eIF4G protein levels, we investigated effects of FKBP7 on eIF4F complex formation using PLA. Docetaxel treatment led to decreased formation of the eIF4E-eIF4G complex in Dtx-sensitive IGR-CaP1 cells (Fig. 5F). Strikingly, but consistently with other studies showing that eIF4E-eIF4G formation determines the sensitivity to anti-cancer targeted therapies (24), this effect was not observed in the IGR-CaP1-Dtx-resistant cell line (Fig. 5F). By affecting the level of eIF4G, siRNA-mediated FKBP7 depletion induced decreased eIF4E–eIF4G complex formation in resistant cells after docetaxel treatment (Fig. 5F). Thus, the reduction of FKBP7 and subsequent decrease in eIF4G level altered the global translation level (Supplementary Fig. S6B), and mimicking this reduction of eIF4G level with eIF4G knock-down equally decreased eIF4F assembly and eIF4G level (Supplementary Fig. S6E). Therefore FKBP7, which is up-regulated in chemoresistant cells, could increase eIF4F complex activity by directly upregulating eIF4G protein levels, leading to hyper-activation of cap-dependent translation and subsequent cell survival after taxane treatment. FKBP7 stabilized eIF4F complex formation after taxane treatment and thus could be a novel eIF4F regulator.

Targeting chemoresistant prostate cancer cells with small molecule inhibitors of eIF4A

As FKBP7 regulates eIF4F complex formation, we first target eIF4F using eIF4G-targeted siRNA before docetaxel treatment on two chemoresistant cell lines (with different androgen-receptor expression). EIF4G silencing provoked a marked cytotoxic effect 5 days after transfection. When combined with docetaxel, chemosensitization was further observed in Dtx-R 22RV1 cells (IC_{50}=62nM with siNT and IC_{50}=23nM with si4G) (Fig. 6A). We next tested three small eIF4F inhibitors (silvestrol, FL3, FL23)

which are reported to target eIF4F complex by inhibiting helicase eIF4A (24,27–29). Silvestrol induced a cytotoxic effect in the A375 melanoma cell line (24), but showed no effect on IGR-CaP1-Dtx-R cells (Fig. 6B), maybe because silvestrol is a Pgp drug efflux pump substrate (30) which is highly expressed in IGR-CaP1-Dtx-R cells (Supplementary Fig. S7A). In contrast, Docetaxel-resistant IGR-CaP1 and 22RV1 cells were sensitive to low doses of FL3 (IC_{50}=19nM and 14nM, respectively) and FL23 (IC_{50}=17nM and 7nM, respectively) (Fig. 6C). Parental cells were sensitive to the same order of flavagline concentrations. FL3 and FL23 translation inhibitors both target eIF4A, but are not Pgp substrates (31). Their IC_{50} values were lower than those observed in melanoma A375 cells (IC_{50}=35 and 25nM, respectively) (Supplementary Fig. S7C). Results showed that FL3 and FL23 were able to kill parental and chemoresistant cells, but no synergy was observed when they were used in combination with docetaxel in resistant cells (Supplementary Fig. S7B-C). We confirmed their cytotoxic effect on parental, Dtx-R and Cbx-R cell lines, as shown by the induction of PARP cleavage (Fig. 6D). FL3 and FL23 did not lead to apoptosis of RPE-1 cells (Fig. 6D), thus reinforcing the interest of targeting eIF4A in prostate cancer.

DISCUSSION

Resistance to chemotherapy represents a major challenge (32,33). Understanding chemoresistance mechanisms and identifying biomarkers is crucial for developing new therapeutic strategies and overcoming drug resistance. In this study, we made the unprecedented observation that FKBP7 is an important determinant of prostate cancer cell response to taxanes. The acquisition of taxane resistance after long term-treatment of prostate cancer cells with docetaxel or cabazitaxel correlates with increased FKBP7 levels. Identification of the FKBP7 signaling network allowed us to link the participation of FKBP7 in chemoresistance to the initiation step of protein translation (eIF4F translation initiation complex). Using eIF4A inhibitors at nanomolar concentrations may help to circumvent docetaxel and cabazitaxel resistance in two prostate cancer chemoresistant cell lines.

Several FKBP proteins have been shown to participate in cancer progression and chemoresistance (7). FKBP5 regulates steroid receptor activation and prostate cancer progression (34). Its expression levels correlate with tumor-cell sensitivity to chemotherapeutic agents (35), and it negatively regulates Akt kinase, thus increasing chemosensitivity (36). FKBP5 is also involved in resistance to anthracycline in malignant melanoma (37) and in taxol resistance in ovarian cancer cells (38). FKBP5 overexpressed after cells had been treated with microtubule-targeting agents, but this was not observed with DNA-damaging agents such as cisplatin (38). This specificity to microtubule-targeting agents may be related to the regulatory role of FKBPs on the cytoskeletal proteins observed for FKBP4 and FKBP5 (10). Other FKBPs such as FKBPL are known to have therapeutic and biomarker potential in cancer (39). The implication of endoplasmic reticulum FKBPs in carcinogenesis has been reported for FKBP10 (40–42) and FKBP14 (43,44).

Our study revealed the functional role of FKBP7 chaperone in docetaxel and cabazitaxel resistance in prostate cancer, which is observed in AR-positive and AR-negative cells, and is independent of ABCB1/MDR1 drug efflux pump expression. Our clinical data showed that high FKBP7 expression is more frequent in tumors *versus* normal tissues, and correlates with a lower time-to-recurrence in patients receiving taxane neoadjuvant chemotherapy. High levels of FKBP7 correlate with a bad prognosis, which suggests that FKBP7 expression could be a relevant marker of taxane-resistance. Pre-clinical evidence in a docetaxel-resistant mouse model confirmed that FKBP7 expression sustained taxane-resistant prostate cancer cell growth. Therefore, our results implicate a previously uncharacterized member of the peptidyl-prolyl isomerase (PPIase) family in the mechanism of resistance to microtubule-targeting agents.

Although high expression of FKBP7 is observed both in non-cancerous and chemoresistant cells, FKBP7 silencing triggers cell death in taxane-resistant tumor cells only, suggesting that the survival of resistant cells may be attributed to a novel function of FKBP7. The comparison of resistant and non-cancerous cells in a large proteomic approach allowed us to identify eukaryotic translational initiation factor and mTOR pathways as the main FKBP7 regulation networks. These pathways are

deregulated in resistant tumor cells *versus* normal cells. We also identified the eIF4G component of the eukaryotic initiation factor eIF4F as a major downstream target of FKBP7 and showed that FKBP7-eIF4G interaction controls the eIF4G protein level. Translation initiation is a highly regulated biological process hijacked by tumor cells to increase the protein synthesis rate for specific genes and promote cell survival. EIF4G is a large scaffolding protein that binds eIF4A helicase and eIF4E cap-binding protein to form the heterotrimeric eIF4F complex for mRNA translation. Evidence showed that increased eIF4F activity contributes to the malignant transformation process via increased translation of a limited set of pro-oncogenic mRNA transcripts (45). As described for the *cis-trans* prolyl isomerase Pin1 (46), the regulation of eIF4G level in resistant cells may be attributed to the PPIase activity of FKBP7 which may act as a dynamic switch allowing the maintenance of eIF4G in an activated but unstable conformation. This acceleration of isomerization may account for high eIF4G level in resistant cells. When FKBP7 is decreased by RNAi silencing, eIF4G is expressed at a low level but the protein seems to be more stable. This increased stability, which might be part of a feed-back loop to overcome the decreased level of eIF4G, may be achieved by a basal chaperone activity of FKBP7. Thus, our data suggest that chemoresistant cell survival may be attributed to over-stimulation of eIF4F, one of the downstream effectors of the Akt-mTOR pathway, mediated by FKBP7 overexpression (Supplementary Fig. S7D).

We showed that FKBP7 plays an important role in survival networks protecting cancer cells against therapeutic agents, so FKBP7 could be an interesting target in prostate cancer. No structural analysis of the full-length FKBP7 protein is currently available for the design of inhibitory molecules, and although screening strategies have been developed to discover new drugs inhibiting FKBP activity, designing isoform specific inhibitors is still challenging (47). Thus, we will now aim our research towards the design of small molecule ligands with FKBP7 specificity. Discovery of the FKBP7-eIF4G interaction led us to assess the efficacy of inhibitors directly targeting the eIF4F complex. We believe that targeting translation machinery is a promising strategy for minimizing acquired resistance (45).

386 We tested silvestrol, an eIF4A inhibitor that is known to provide therapeutic benefits in prostate
387 cancer xenografts (28). Unfortunately, silvestrol showed no obvious efficacy towards docetaxel-
388 resistant IGR-CaP1 cell proliferation, which could be attributed to high expression of ABCB/MDR1 in
389 this model. In contrast, flavaglines FL3 and FL23, which also target eIF4A, are highly cytotoxic in
390 docetaxel-resistant models. These synthetic compounds (48,49) are known to overcome multidrug
391 resistance *in vitro* (31) and alleviate resistance to vemurafemib in melanoma (24).

392 Our findings open a new avenue in the field of chemoresistance, and our study reveals the critical
393 role played by chaperone FKBP7 in acquired taxane-resistance in prostate cancer and its potential for
394 development as a predictor of chemoresistance. By targeting FKBP7 or the eIF4F complex, we also
395 found novel therapeutic strategies that would help to manage taxane-resistant prostate cancer.

396

ACKNOWLEDGMENTS

We gratefully thank A. Lescure and S. Tessier, who are Biophenics staff, the platform of preclinical evaluation AMMICA, the bioinformatic Core Facility, the Development in Pathology Group (UMR981), and S. Shen (UMR981). We thank and pay tribute to Vasily Ogryzko (UMR8126), who gave us precious help with proteomics but passed away before this publication. RWPE-1 was a kind gift from G. Mouchiroud (University Claude Bernard, Lyon), HK-2 was provided by S. Gad-Lapiteau (UMR1186, Villejuif), and HUVEC was provided by S. Rodrigues-Ferreira (UMR981, Villejuif). We also thanks Joanna Moore, ELS (Citoxlab France), for assistance in the preparation of the manuscript. MGa was supported by the Idex Paris-Saclay fellowship and the Association pour la Recherche sur les tumeurs de la Prostate (ARTP). NJ-PM, MB and NEK were supported by the PARRAINAGE CHERCHEUR charity program of Gustave Roussy.

This work was supported by grants from: INSERM, the Université Paris-Sud11, the grant PAIR PROSTATE program n°2010-1-PRO-03 from the INCA, the ARC Foundation, the Ligue contre le cancer, the ECOS-Sud A10S03 program, AMGEN, the Paris Alliance of Cancer Research Institutes program, “Investissements d’Avenir” an initiative of the French Government implemented by ANR under reference ANR-11-PHUC-002, Taxe d'apprentissage Gustave Roussy P21NNGE for genomic and 2014MG for proteomic analyses, and Terry Fox New Frontiers Program Project Grant TFF116129.

AUTHOR CONTRIBUTIONS

MGa, N J-PM, MB, CG, NEK, VO, NAN, LF, EDN, SL, and ALP performed the experiments and analyzed data; FC performed bioinformatics analysis; JC, FP, MG, YL, SV, LD and KF provided expertise and feedback; MG and LD provided useful reagents; AC and KF secured funding for the project, MGa and AC wrote the manuscript; AC conceived and supervised the project.

REFERENCES

1. Ischia J, Saad F, Gleave M. The promise of heat shock protein inhibitors in the treatment of castration resistant prostate cancer. Curr Opin Urol. 2013;23:194–200.

2. Lamoureux F, Thomas C, Yin M-J, Fazli L, Zoubeidi A, Gleave ME. Suppression of heat shock protein 27 using OGX-427 induces endoplasmic reticulum stress and potentiates heat shock protein 90 inhibitors to delay castrate-resistant prostate cancer. Eur Urol. 2014;66:145–55.

3. Hurwitz M. Chemotherapy in Prostate Cancer. Curr Oncol Rep. 2015;17:44.

4. James ND, Sydes MR, Clarke NW, Mason MD, Dearnaley DP, Spears MR, et al. Addition of docetaxel, zoledronic acid, or both to first-line long-term hormone therapy in prostate cancer (STAMPEDE): survival results from an adaptive, multiarm, multistage, platform randomised controlled trial. Lancet (London, England). 2016;387:1163–77.

5. Seruga B, Ocana A, Tannock IF. Drug resistance in metastatic castration-resistant prostate cancer. Nat Rev Clin Oncol. 2011;8:12–23.

6. Mahon KL, Henshall SM, Sutherland RL, Horvath LG. Pathways of chemotherapy resistance in castration-resistant prostate cancer. Endocr Relat Cancer. 2011;18:R103-123.

7. Solassol J, Mange A, Maudelonde T. FKBP family proteins as promising new biomarkers for cancer. Curr Opin Pharmacol. 2011;11:320–5.

8. Zoubeidi A, Gleave M. Small heat shock proteins in cancer therapy and prognosis. Int J Biochem Cell Biol. 2012;44:1646–56.

9. Bierer BE, Mattila PS, Standaert RF, Herzenberg LA, Burakoff SJ, Crabtree G, et al. Two distinct signal transmission pathways in T lymphocytes are inhibited by complexes formed between an immunophilin and either FK506 or rapamycin. Proc Natl Acad Sci U S A. 1990;87:9231–5.

10. Cioffi DL, Hubler TR, Scammell JG. Organization and function of the FKBP52 and FKBP51 genes. Curr Opin Pharmacol. 2011;11:308–13.

11. Nakamura T, Yabe D, Kanazawa N, Tashiro K, Sasayama S, Honjo T. Molecular cloning, characterization, and chromosomal localization of FKBP23, a novel FK506-binding protein with Ca2+-binding ability. Genomics. 1998;54:89–98.

12. Zhang X, Wang Y, Li H, Zhang W, Wu D, Mi H. The mouse FKBP23 binds to BiP in ER and the binding of C-terminal domain is interrelated with Ca2+ concentration. FEBS Lett. 2004;559:57–60.

13. Nakouzi N Al, Cotteret S, Commo F, Gaudin C, Rajpar S, Dessen P, et al. Targeting CDC25C, PLK1 and CHEK1 to overcome Docetaxel resistance induced by loss of LZTS1 in prostate cancer. Oncotarget. 2014;5:667–78.

14. Giraldo J, Vivas NM, Vila E, Badia A. Assessing the (a)symmetry of concentration-effect curves: empirical versus mechanistic models. Pharmacol Ther. 2002;95:21–45.

15. Yoav Benjamini YH. Controlling the False Discovery Rate: A Practical and Powerful Approach to Multiple Testing. J R Stat Soc. 1995;57:289–300.

16. Shevchenko A, Tomas H, Havlis J, Olsen J V, Mann M. In-gel digestion for mass spectrometric

characterization of proteins and proteomes. Nat Protoc. 2006;1:2856–60.

17. Chauchereau A, Al Nakouzi N, Gaudin C, Le Moulec S, Compagno D, Auger N, et al. Stemness markers characterize IGR-CaP1, a new cell line derived from primary epithelial prostate cancer. Exp Cell Res. 2011;317:262–75.

18. Gifford JB, Huang W, Zeleniak AE, Hindoyan A, Wu H, Donahue TR, et al. Expression Of GRP78, Master Regulator Of The Unfolded Protein Response, Increases Chemoresistance In Pancreatic Ductal Adenocarcinoma. Mol Cancer Ther. 2016;

19. Roller C, Maddalo D. The Molecular Chaperone GRP78/BiP in the Development of Chemoresistance: Mechanism and Possible Treatment. Front Pharmacol. 2013;4:10.

20. Kuruma H, Matsumoto H, Shiota M, Bishop J, Lamoureux F, Thomas C, et al. A Novel Antiandrogen, Compound 30, Suppresses Castration-Resistant and MDV3100-Resistant Prostate Cancer Growth In Vitro and In Vivo. Mol Cancer Ther. 2013;12:567–76.

21. Yamamoto Y, Loriot Y, Beraldi E, Zhang F, Wyatt AW, Nakouzi NA, et al. Generation 2.5 Antisense Oligonucleotides Targeting the Androgen Receptor and Its Splice Variants Suppress Enzalutamide-Resistant Prostate Cancer Cell Growth. Clin Cancer Res. 2015;21:1675–87.

22. Grasso CS, Wu Y-M, Robinson DR, Cao X, Dhanasekaran SM, Khan AP, et al. The mutational landscape of lethal castration-resistant prostate cancer. Nature. 2012;487:239–43.

23. Cencic R, Hall DR, Robert F, Du Y, Min J, Li L, et al. Reversing chemoresistance by small molecule inhibition of the translation initiation complex eIF4F. Proc Natl Acad Sci U S A. 2011;108:1046–51.

24. Boussemart L, Malka-Mahieu H, Girault I, Allard D, Hemmingsson O, Tomasic G, et al. eIF4F is a nexus of resistance to anti-BRAF and anti-MEK cancer therapies. Nature. 2014;513:105–9.

25. Robert F, Roman W, Bramoullé A, Fellmann C, Roulston A, Shustik C, et al. Translation initiation factor eIF4F modifies the dexamethasone response in multiple myeloma. Proc Natl Acad Sci U S A. 2014;111:13421–6.

26. Zindy P, Bergé Y, Allal B, Filleron T, Pierredon S, Cammas A, et al. Formation of the eIF4F translation-initiation complex determines sensitivity to anticancer drugs targeting the EGFR and HER2 receptors. Cancer Res. 2011;71:4068–73.

27. Bordeleau M-E, Robert F, Gerard B, Lindqvist L, Chen SMH, Wendel H-G, et al. Therapeutic suppression of translation initiation modulates chemosensitivity in a mouse lymphoma model. J Clin Invest. 2008;118:2651–60.

28. Cencic R, Carrier M, Galicia-Vázquez G, Bordeleau M-E, Sukarieh R, Bourdeau A, et al. Antitumor activity and mechanism of action of the cyclopenta[b]benzofuran, silvestrol. PLoS One. 2009;4:e5223.

29. Chambers JM, Lindqvist LM, Webb A, Huang DCS, Savage GP, Rizzacasa MA. Synthesis of biotinylated episilvestrol: highly selective targeting of the translation factors eIF4AI/II. Org Lett. 2013;15:1406–9.

30. Gupta S V, Sass EJ, Davis ME, Edwards RB, Lozanski G, Heerema NA, et al. Resistance to the translation initiation inhibitor silvestrol is mediated by ABCB1/P-glycoprotein overexpression in acute lymphoblastic leukemia cells. AAPS J. 2011;13:357–64.

31. Thuaud F, Bernard Y, Türkeri G, Dirr R, Aubert G, Cresteil T, et al. Synthetic analogue of rocaglaol displays a potent and selective cytotoxicity in cancer cells: involvement of apoptosis inducing factor and caspase-12. J Med Chem. 2009;52:5176–87.

32. Rebucci M, Michiels C. Molecular aspects of cancer cell resistance to chemotherapy. Biochem Pharmacol. 2013;85:1219–26.

33. Zhang W, Meng Y, Liu N, Wen X-F, Yang T. Insights into Chemoresistance of Prostate Cancer. Int J Biol Sci. 2015;11:1160–70.

34. Storer CL, Dickey CA, Galigniana MD, Rein T, Cox MB. FKBP51 and FKBP52 in signaling and disease. Trends Endocrinol Metab. 2011;22:481–90.

35. Li L, Fridley B, Kalari K, Jenkins G, Batzler A, Safgren S, et al. Gemcitabine and cytosine arabinoside cytotoxicity: association with lymphoblastoid cell expression. Cancer Res. 2008;68:7050–8.

36. Pei H, Li L, Fridley BL, Jenkins GD, Kalari KR, Lingle W, et al. FKBP51 affects cancer cell response to chemotherapy by negatively regulating Akt. Cancer Cell. 2009;16:259–66.

37. Romano MF, Avellino R, Petrella A, Bisogni R, Romano S, Venuta S. Rapamycin inhibits doxorubicin-induced NF-kappaB/Rel nuclear activity and enhances the apoptosis of melanoma cells. Eur J Cancer. 2004;40:2829–36.

38. Sun N-K, Huang S-L, Chang P-Y, Lu H-P, Chao CC-K. Transcriptomic profiling of taxol-resistant ovarian cancer cells identifies FKBP5 and the androgen receptor as critical markers of chemotherapeutic response. Oncotarget. 2014;5:11939–56.

39. Robson T, James IF. The therapeutic and diagnostic potential of FKBPL; a novel anticancer protein. Drug Discov Today. 2012;17:544–8.

40. Paulo P, Ribeiro FR, Santos J, Mesquita D, Almeida M, Barros-Silva JD, et al. Molecular subtyping of primary prostate cancer reveals specific and shared target genes of different ETS rearrangements. Neoplasia. 2012;14:600–11.

41. Olesen SH, Christensen LL, Sørensen FB, Cabezón T, Laurberg S, Orntoft TF, et al. Human FK506 binding protein 65 is associated with colorectal cancer. Mol Cell Proteomics. 2005;4:534–44.

42. Quinn MCJ, Wojnarowicz PM, Pickett A, Provencher DM, Mes-Masson A-M, Davis EC, et al. FKBP10/FKBP65 expression in high-grade ovarian serous carcinoma and its association with patient outcome. Int J Oncol. 2013;42:912–20.

43. Lu M, Miao Y, Qi L, Bai M, Zhang J, Feng Y. RNAi-Mediated Downregulation of FKBP14 Suppresses the Growth of Human Ovarian Cancer Cells. Oncol Res. 2016;23:267–74.

44. Huang Z, Li J, Du S, Tang Y, Huang L, Xiao L, et al. FKBP14 overexpression contributes to osteosarcoma carcinogenesis and indicates poor survival outcome. Oncotarget. 2016;

45. Bhat M, Robichaud N, Hulea L, Sonenberg N, Pelletier J, Topisirovic I. Targeting the translation machinery in cancer. Nat Rev Drug Discov. 2015;14:261–78.

46. Lu KP, Finn G, Lee TH, Nicholson LK. Prolyl cis-trans isomerization as a molecular timer. Nat Chem Biol. 2007;3:619–29.

47. Blackburn EA, Walkinshaw MD. Targeting FKBP isoforms with small-molecule ligands. Curr

Opin Pharmacol. 2011;11:365–71.

48. Thuaud F, Ribeiro N, Gaiddon C, Cresteil T, Désaubry L. Novel flavaglines displaying improved cytotoxicity. J Med Chem. 2011;54:411–5.

49. Ribeiro N, Thuaud F, Bernard Y, Gaiddon C, Cresteil T, Hild A, et al. Flavaglines as potent anticancer and cytoprotective agents. J Med Chem. 2012;55:10064–73.

FIGURE LEGENDS

Figure 1

FKBP7 is upregulated during the progression of chemoresistant CRPC. **A**, Immunoblot of FKBP7 protein expression in RWPE-1 non-cancerous prostate cells, parental (S) IGR-CaP1, PC3, LNCaP and 22RV1, docetaxel-resistant cells (Dtx-R) and cabazitaxel-resistant cells (Cbx-R) (loading control: actin. FKBP7). Protein level was quantified with Image Lab software. FKBP7 in resistant cells is expressed relative to parental cell line. *indicates non-specific band. **B**, Immunoblot showing FKBP7 protein level in various parental cells after treatment with 10nM Docetaxel or Cabazitaxel for 24h, 48h, 72h and 120h. Actin or Hsc70 are the loading controls. **C**, Immunoblot showing FKBP7 protein level in parental (S) or docetaxel-resistant (R) LNCaP cells in comparison with LNCaP-derived models that are responsive (V16D) or resistant (49F and 42D) to enzalutamide. Hsc70 was the loading control. **D**-Left, Representative immunohistochemistry images of FKBP7 staining in prostate tissues. Scale bars: 200µm (top). **D**-Right, Quantification of FKBP7 protein level in benign prostate tissue and tumor. Chi-square test p=0.0001. FKBP7 low corresponds to scores 0 and 1; FKBP7 high corresponds to scores 2 and 3. n=808. **E**, Correlation of FKBP7 expression intensity with recurrence % in 69 patients treated with docetaxel. Fisher's exact test p=0.0059. Events are defined as any recurrence, metastasis or post-surgery death from prostate cancer (baseline: date of surgery). **F**, Kaplan-Meir plot representing recurrence-free survival (RFS) associated with FKBP7 staining in TMA from 69 patients who received docetaxel as neoadjuvant therapy. The association between time-to-recurrence (months) and FKBP7-staining status (high or low), where events are defined as PSA recurrence, metastasis or death from prostate cancer, was calculated with Cox proportional hazard model: Hazard ratio 0.3846 (95% confidence interval: 0.195 to 0.7586); p=0.004 (log rank test).

Figure 2.

SiRNA-mediated knock-down of FKBP7 blocks chemoresistant cell growth and increases apoptosis in resistant cells treated with taxane. **A**, Immunoblot shows FKBP7 knockdown efficiency 48h after

transfection with different siRNA sequences targeting FKBP7 (circles) or siNT (■) (control siRNA) (loading control: actin). Cell viability was determined daily (WST1 assay) after transfection with siRNA. Data are presented as mean ±SD. Data were normalized to control condition without siRNA. **p<0.01;***p<0.0005;****p<0.0001 as determined by two-way ANOVA with Bonferroni posttests. Experiments were performed with docetaxel- or cabazitaxel-resistant cells. **B**, Immunoblots showing cleaved (Cl.) PARP protein (89KDa) in docetaxel- or cabazitaxel-resistant cells after 96h of transfection with siNT, siFK-1 or siFK-2, alone or combined with docetaxel (Dtx) or cabazitaxel (Cbx) treatment for 72h. Chemoresistant cells were treated at their respective maximum resistance dose (Supplementary Fig. S1) (loading control: HSC70)

Figure 3.

FKBP7 silencing reduces tumor growth in a docetaxel-resistant mouse model. **A**, Growth curves of tumors from IGR-CaP1 and IGR-CaP1-Rvivo subcutaneous xenografts after treatment with vehicle (5% glucose solution, ○) or docetaxel (30mg/kg I.P., ●). Data represent the mean ±SD. Mice/group: n=5. Arrows indicate the times of docetaxel injections. ***p<0.001 (two-way ANOVA with Bonferroni posttests). **B-Left**, Proliferation assay. Determination of docetaxel treatment IC_{50} in parental IGR-CaP1 (○) and IGR-CaP-Rvivo (●) cells. Data are presented as mean ±SD. Cell viability is relative to control treatment. **B-Right**, Immunoblot of FKBP7 in IGR-CaP1 (S) and IGR-CaP1-Rvivo cells (loading control: actin). **C**, Immunoblot shows FKBP7 knockdown efficiency after the transduction of IGR-CaP1-Rvivo cells with lentivirus expressing two shRNAs targeting FKBP7 *versus* control shRNA, compared to the parental IGR-CaP1 cells (S). A quantification of FKBP7/actin was performed (Image Lab software). **C-Left**, Average tumor volume ±SEM obtained from xenografts of IGR-CaP1-Rvivo transduced with control shRNA (○) (n=6) or FKBP7-directed shRNAs (● and grey circles) (n=7/group) before treatment. **C-Right**, When tumors reached 450-500mm^3, mice received vehicle or docetaxel. The tumor volume ratio between mice receiving docetaxel and mice receiving vehicle (on days 0 and 21) is presented (shCtrl: n=6/group; shFKBP7s: n=7/group).

Figure 4.

FKBP7 interacts with eukaryotic translation initiation factors **A**, Ingenuity pathway analysis showing the canonical pathways identified with the specific protein partners of FKBP7 in IGR-CaP1-Dtx-R and RPE-1 from global proteomic IP. **B**, Major three pathways deregulated in cells transfected with an siRNA targeting FKBP7 (siFK-2), identified with IPA analysis from SILAC data. Each pathway is associated with a p-value and a Z-score for IGR-CaP1-Dtx-R and RPE-1. **C**, Network showing the protein members of the eIF2, eIF4 and mTOR pathways deregulated by FKBP7 knockdown in IGR-CaP1-Dtx-R and RPE-1 cells. The color represents the fold change of protein expression between siFKBP7 and siNT. **D-Left**, endogenous FKBP7 was immunoprecipitated with the anti-FKBP7 antibody (or IgG as control) in docetaxel-resistant IGR-CaP1 and PC3 cells. Immunoblot showing the eIF4G co-immunoprecipited protein. Input controls (20%) are shown. **D-Right**, eIF4G was immunoprecipitated with the anti-eIF4G antibody (or IgG as control) in docetaxel-resistant IGR-CaP1 and PC3 cells. Immunoblot showing the FKBP7 co-immunoprecipited protein. Input controls (20%) are shown.

Figure 5.

FKBP7 regulates the formation of eIF4F translation initiation complex **A**, Immunoblots showing eIF4G, eIF4A and eIF4E expression in IGR-CaP1-Dtx-R and RPE-1 cells transfected with siRNA control (siNT) or with siFK-1 or siFK-2 (siRNAs targeting FKBP7) (loading controls: HSC70 and actin). **B**, Immunoblots showing eIF4G expression in docetaxel-resistant (Dtx-R) 22RV1 and LNCaP and cabazitaxel-resistant (Cbx-R) IGR-CaP1 and LNCaP cells transfected with siNT, siFK-1 or siFK-2 (loading control: HSC70). The eIF4G/HSC70 ratio was calculated with Image Lab software. **C**, Dtx-R 22RV1 cells transfected with siRNA control (siNT) or with siFK-2 for 48h were treated with 10µm/ml Cycloheximide at the indicated time point. Whole cell extract was collected serially and eIF4G and FKBP7 were detected by immunoblot (loading control: actin). Quantified EIF4G level was plotted. **D**, Immunoblots showing eIF4G knockdown efficiency 48h after transfection with either siRNA targeting eIF4G (sieIF4G) or siRNA control (siNT) in Dtx-R IGR-CaP1 and 22RV1 cells. HSC70 is the loading control. **E**, FKBP7-eIF4G

interaction detected by PLA in IGR-CaP1-Dtx-R and 22RV1-Dtx-R cells. Cells were either untreated or transfected with siNT, siRNA targeting FKBP7 (siFK-2) or siRNA targeting eIF4G (sieIF4G). Scale bars: 20µm. Interactions: red dots, nuclei: blue dots. Interaction dots were quantified (n≥100 cells) and analyzed (general linear model, ***p<0.001). **F-Left**, eIF4E-eIF4G interaction detected by PLA in parental and Dtx-R IGR-CaP1 cells. Cells were either untreated or treated with 5nM of docetaxel for 24h. **F-Right**, eIF4E-eIF4G interactions were detected on Dtx-R IGR-CaP1 cells transfected with siNT, siFK-1 or siFK-2, alone or combined with 5nM of docetaxel for 24h. Scale bars: 20µm. Interactions: red dots, nuclei: blue dots. Interaction dots were quantified (n≥100 cells) and analyzed (general linear model or Wilcoxon rank test, ** p<0.01;*** p<0.001).

Figure 6.

Targeting eIF4F in chemoresistant prostate cancer cells with siRNA or with small molecule inhibitors of eIF4A. **A**, Proliferation assay. Cell viability of Dtx-resistant IGR-CaP1 and 22RV1 cells after 48h transfection with siRNA targeting eIF4G (4G) or control siRNA (siNT) and a further treatment with increasing doses of docetaxel for 72h. Data are presented as mean ±SD. **B,** Cell viability (vs control treatment) of IGR-CaP1-Dtx-R (●) and melanoma A375 cells (○) after 48h of treatment with silvestrol. Data are presented as mean ±SD. **C**, Cell viability (vs control treatment) of docetaxel-resistant (Dtx-R, ●) and parental (○) IGR-CaP1 and 22RV1 cells after 48h of treatment with either flavagline 3 (FL3, left panel) or flavagline 23 (FL23, right panel). Data are presented as mean ±SD. **D**, Immunoblots of cleaved (Cl.) PARP protein (89KDa) in parental, docetaxel- and cabazitaxel-resistant IGR-CaP1 and 22RV1 cells and in RPE-1 cells, either untreated (ctrl), treated for 72h with 10nM docetaxel (Dtx) or 5nM cabazitaxel (Cbx), or treated for 48h with 150nM flavagline FL3 or FL23 (loading control: HSC70).

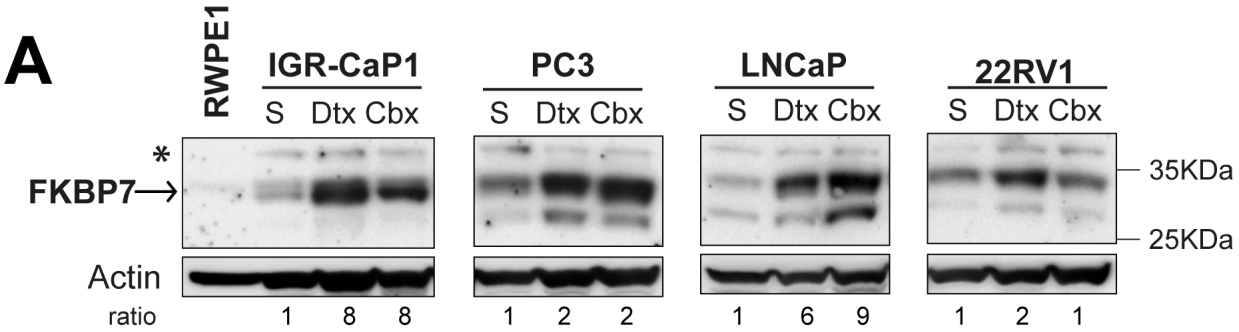

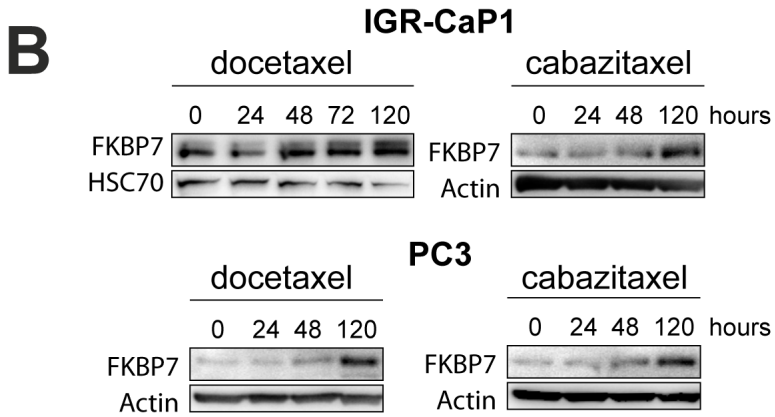

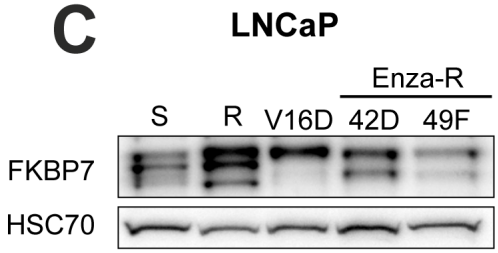

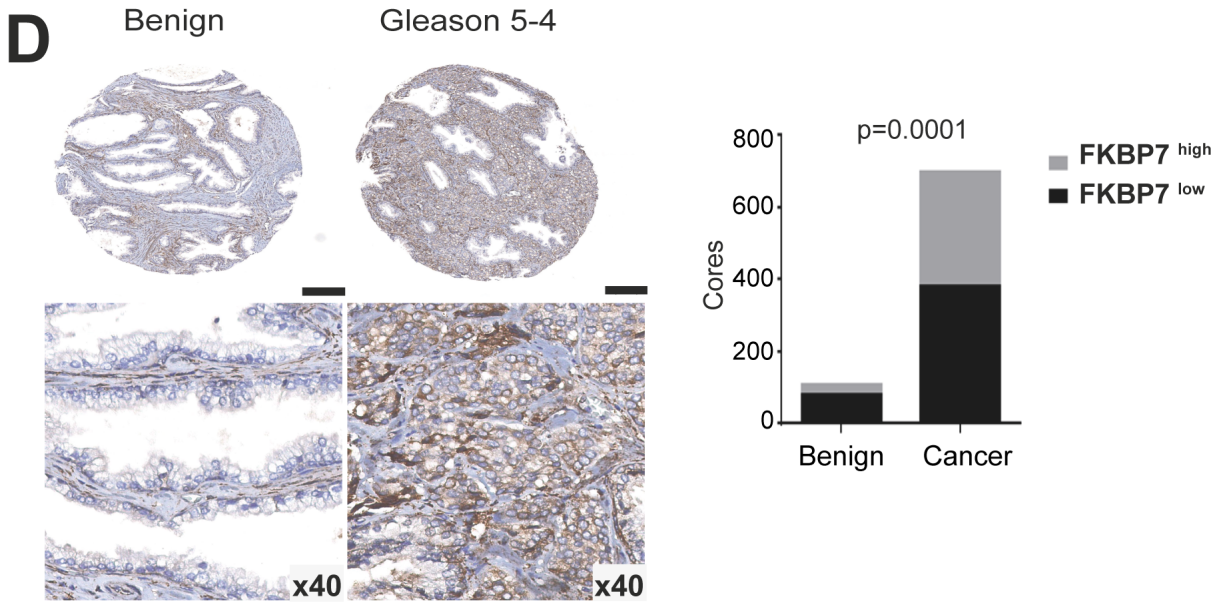

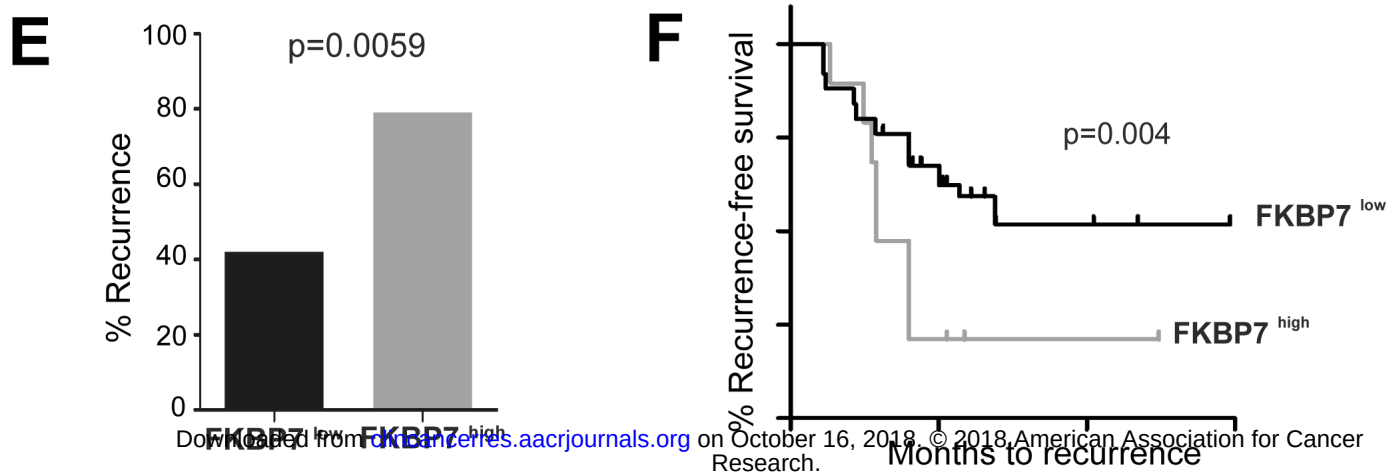

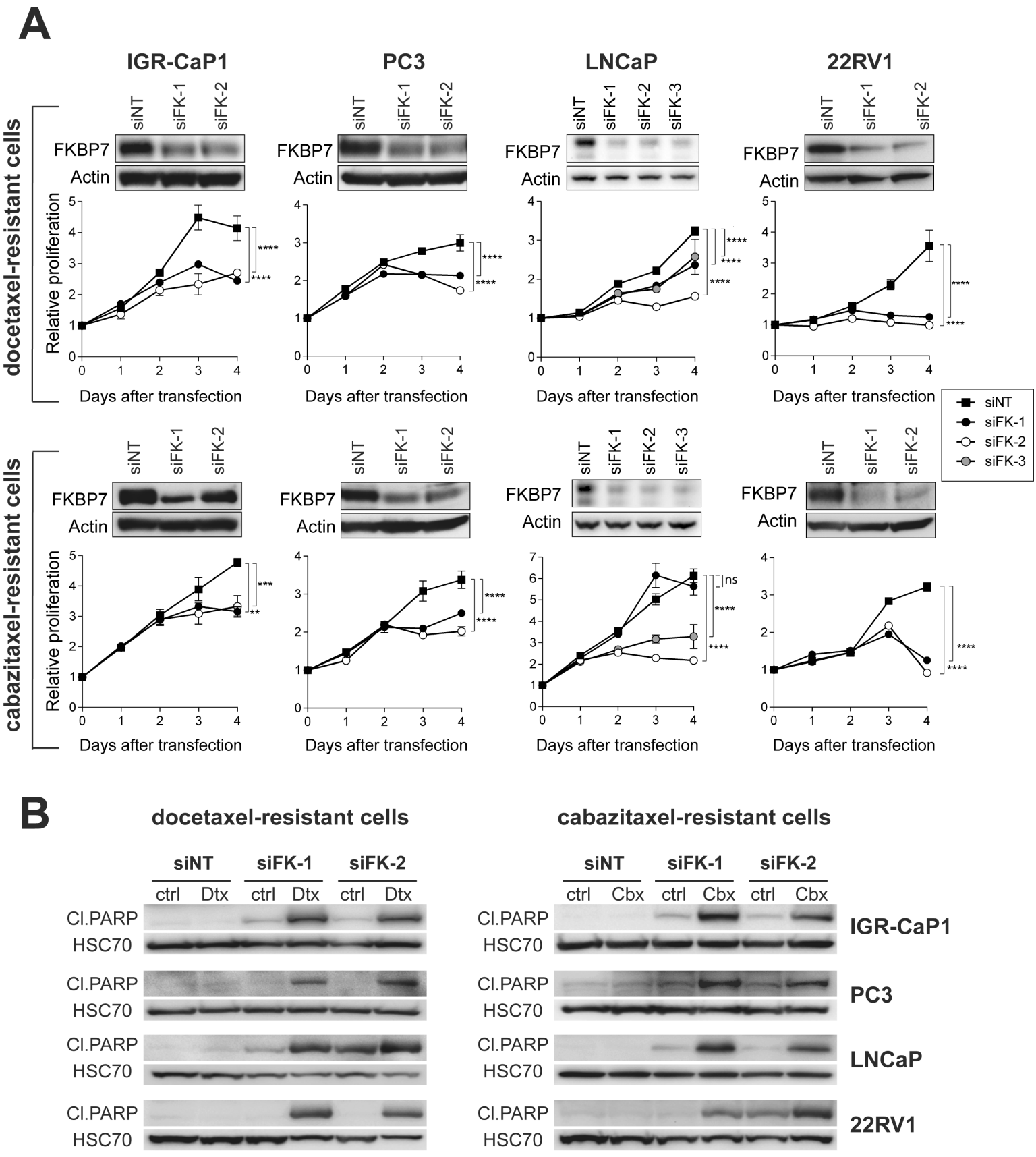

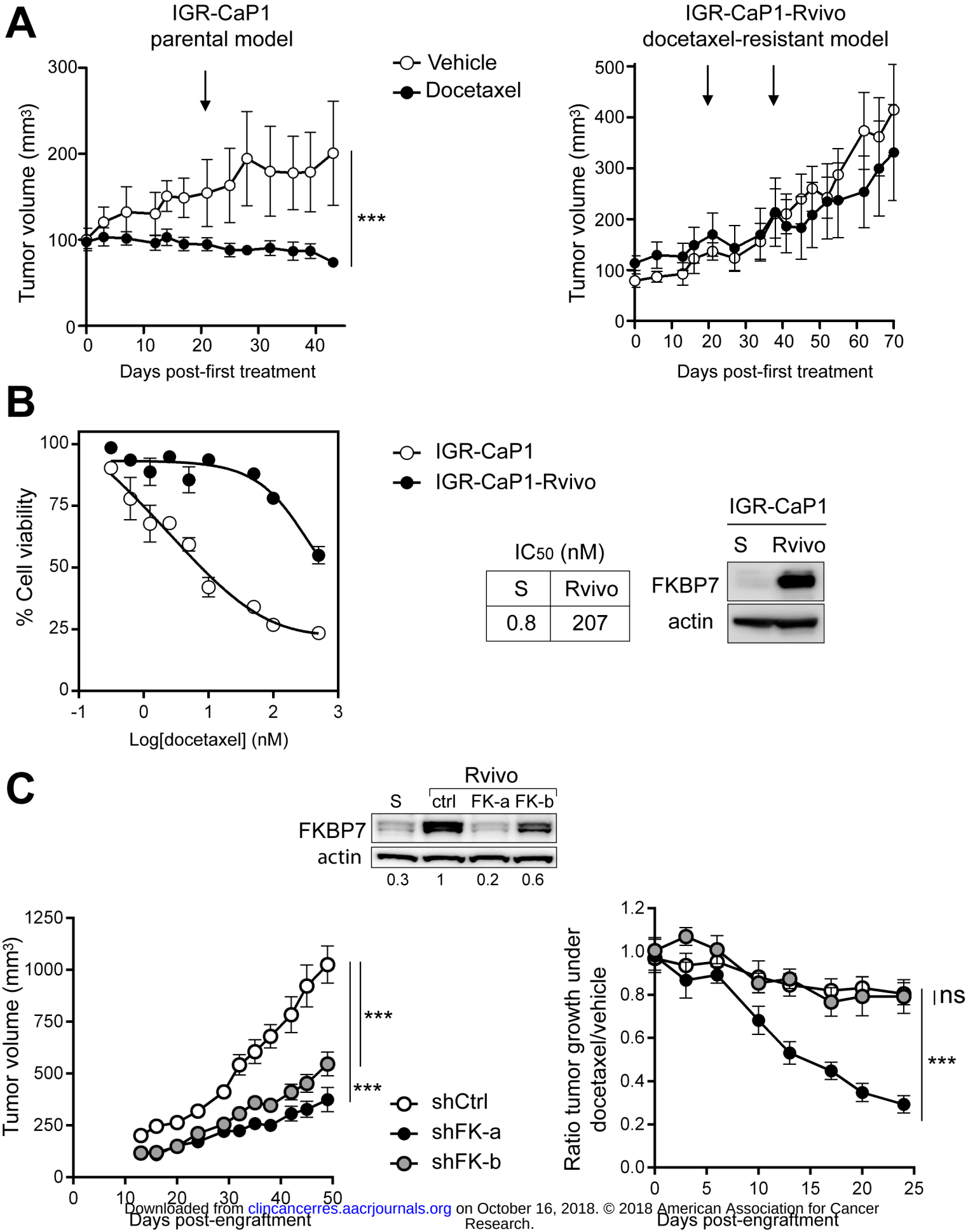

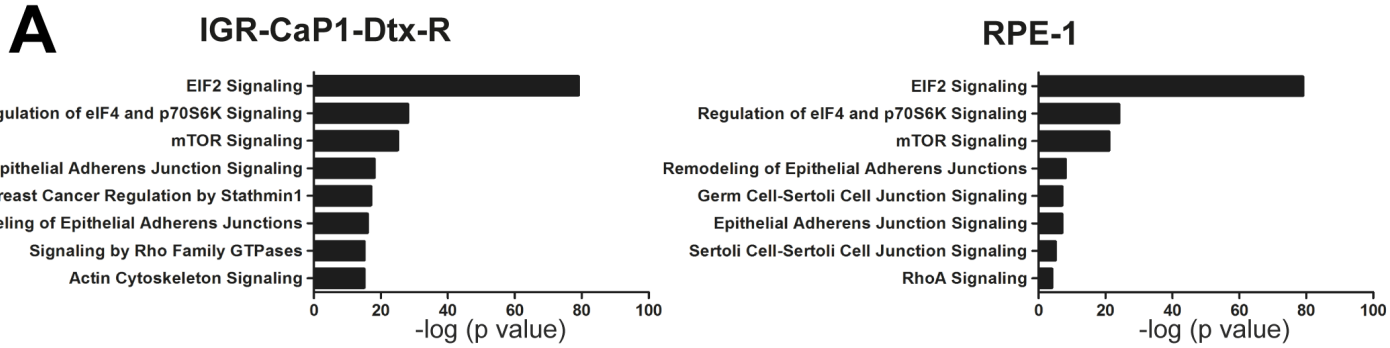

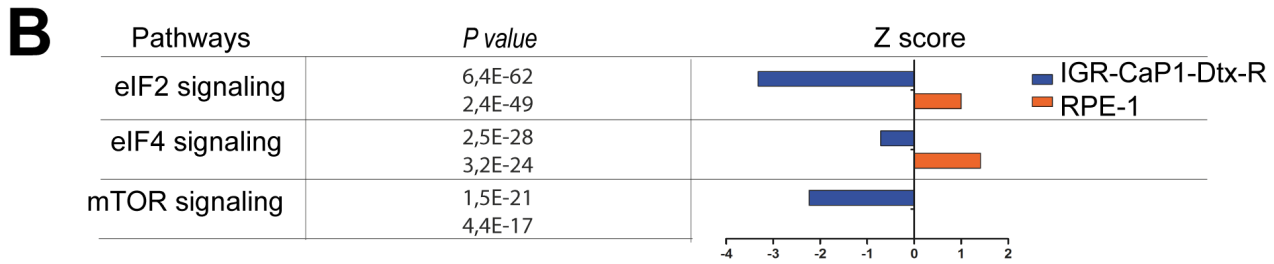

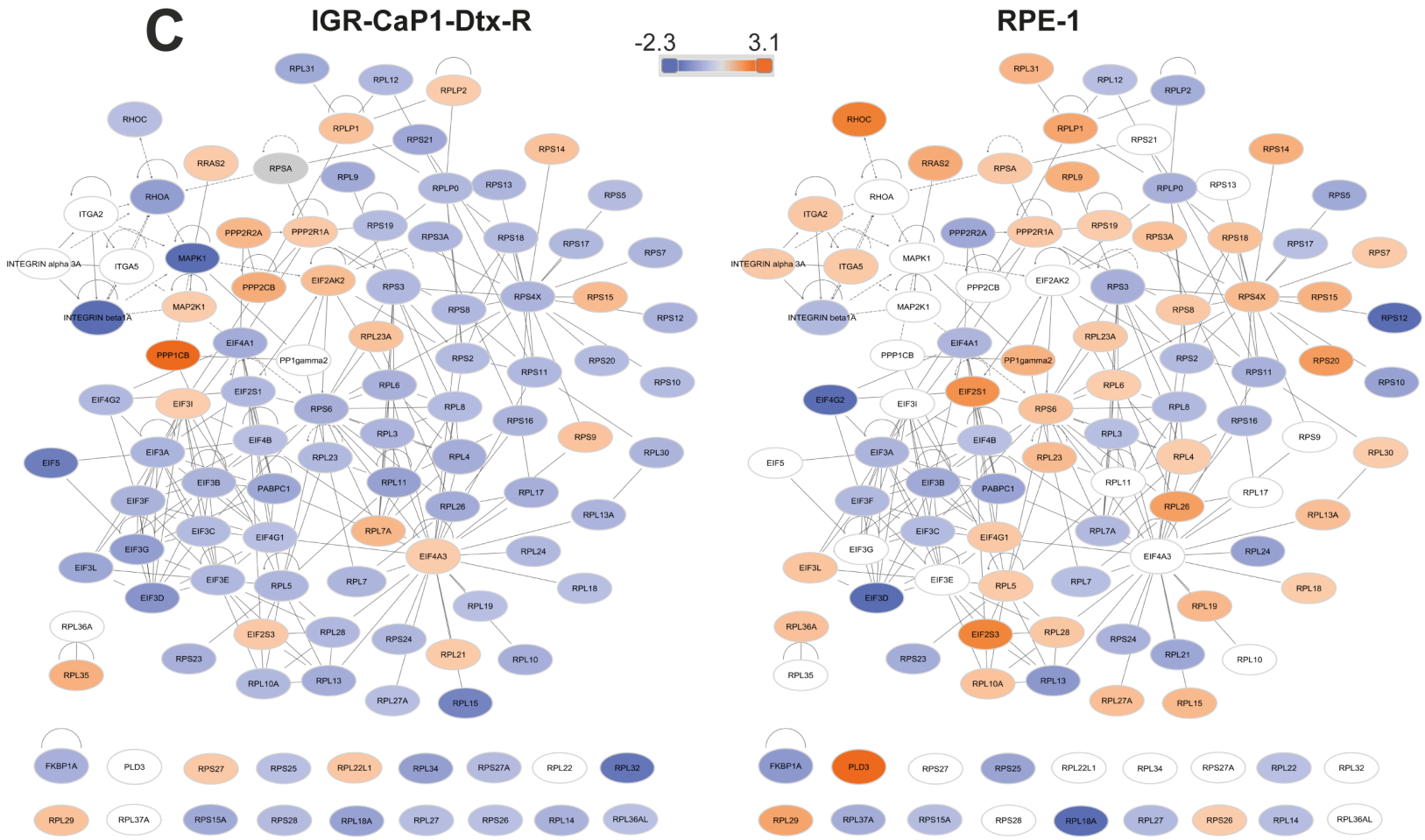

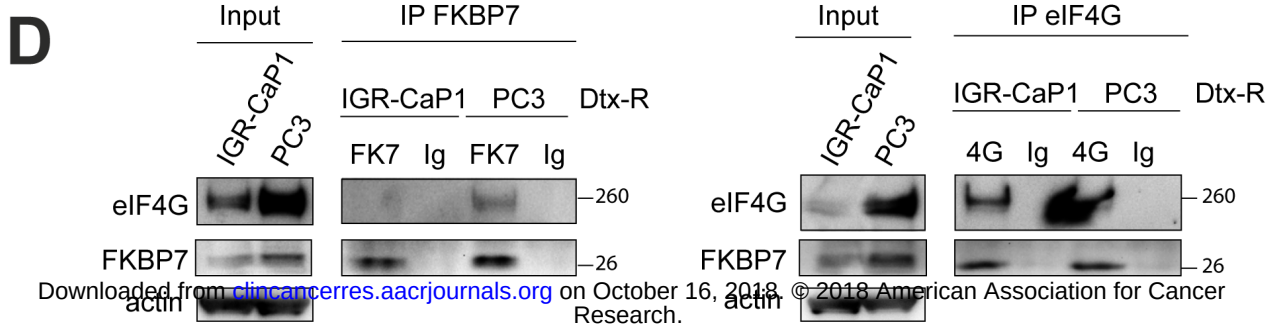

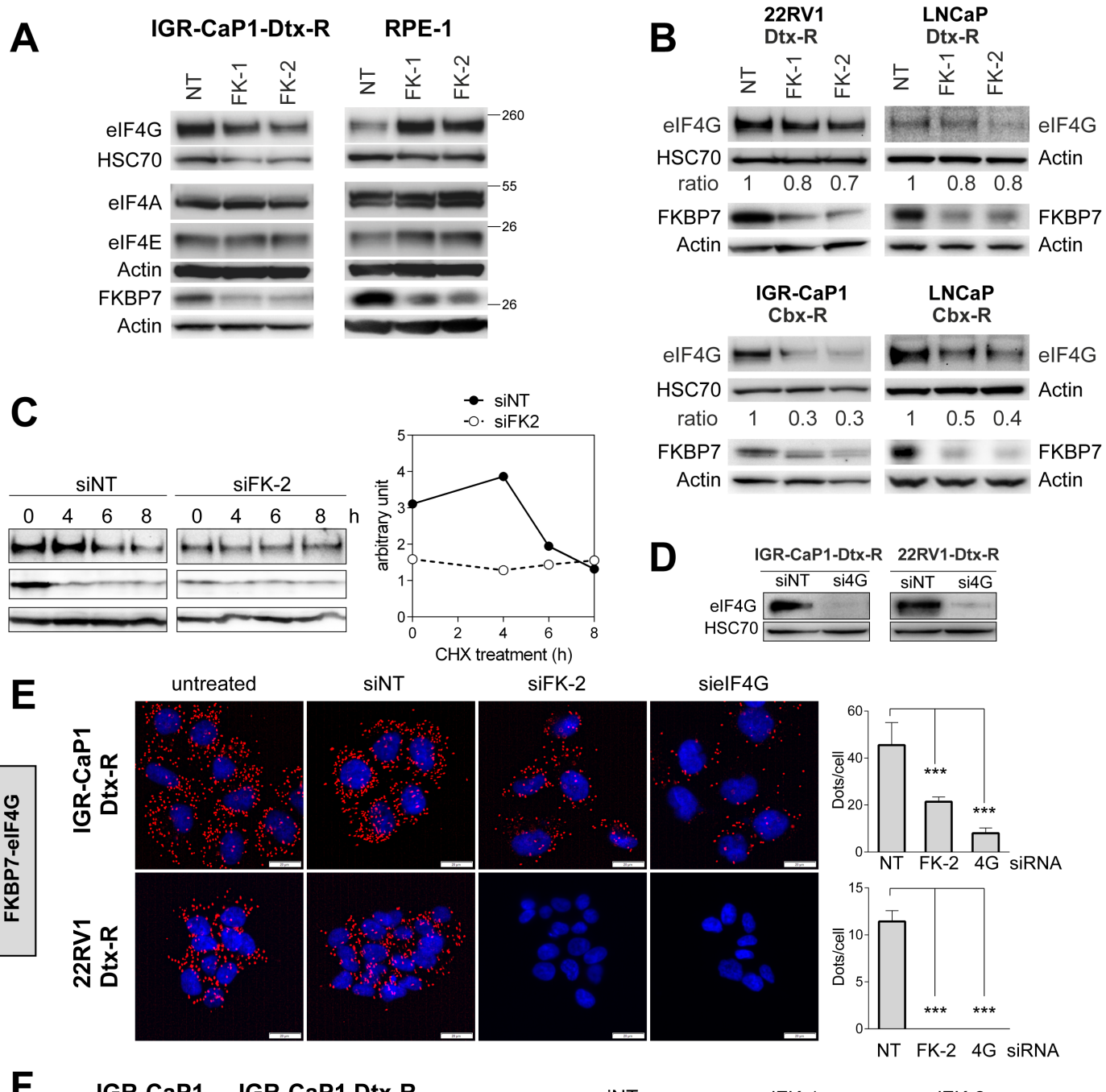

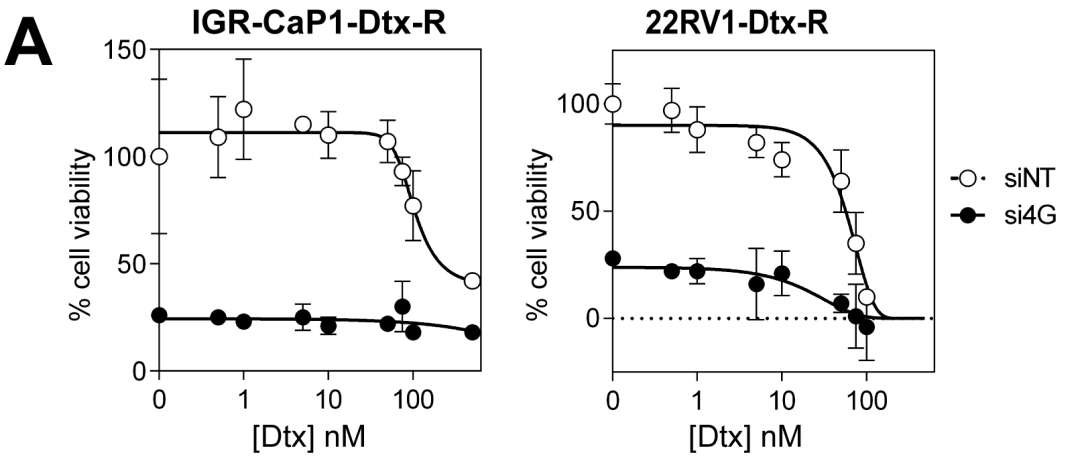

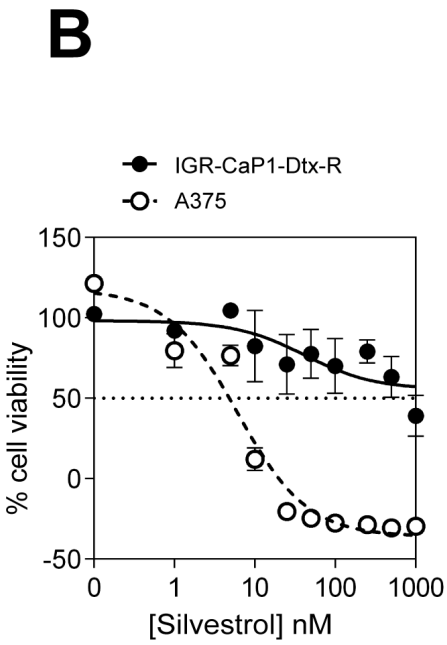

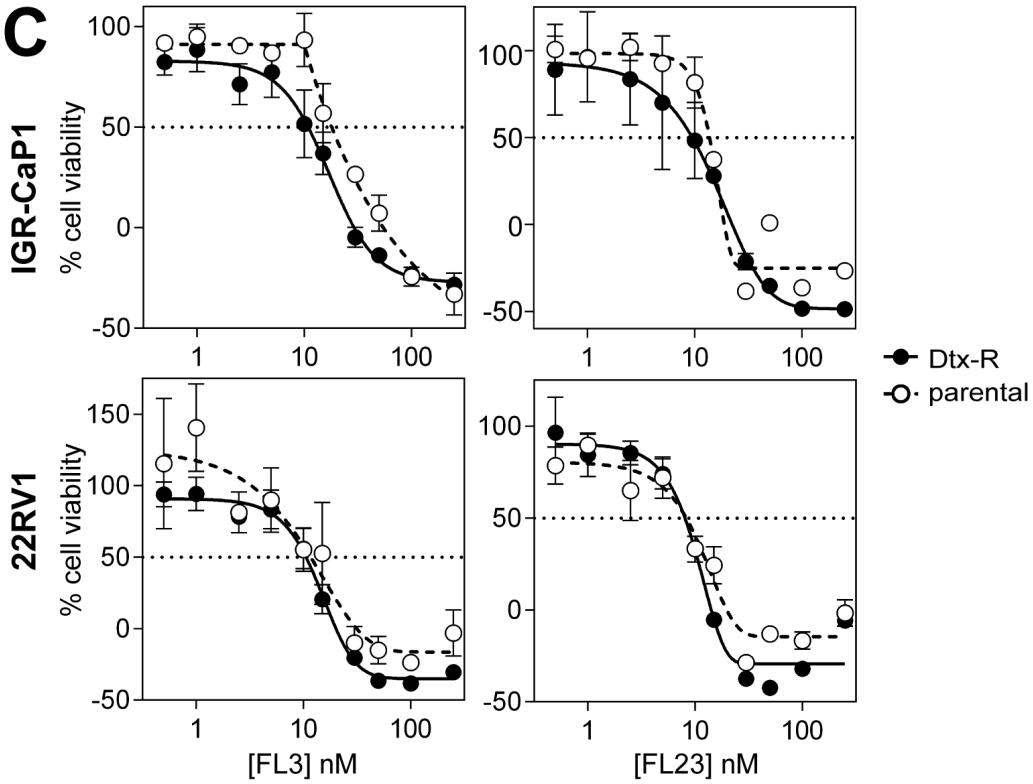

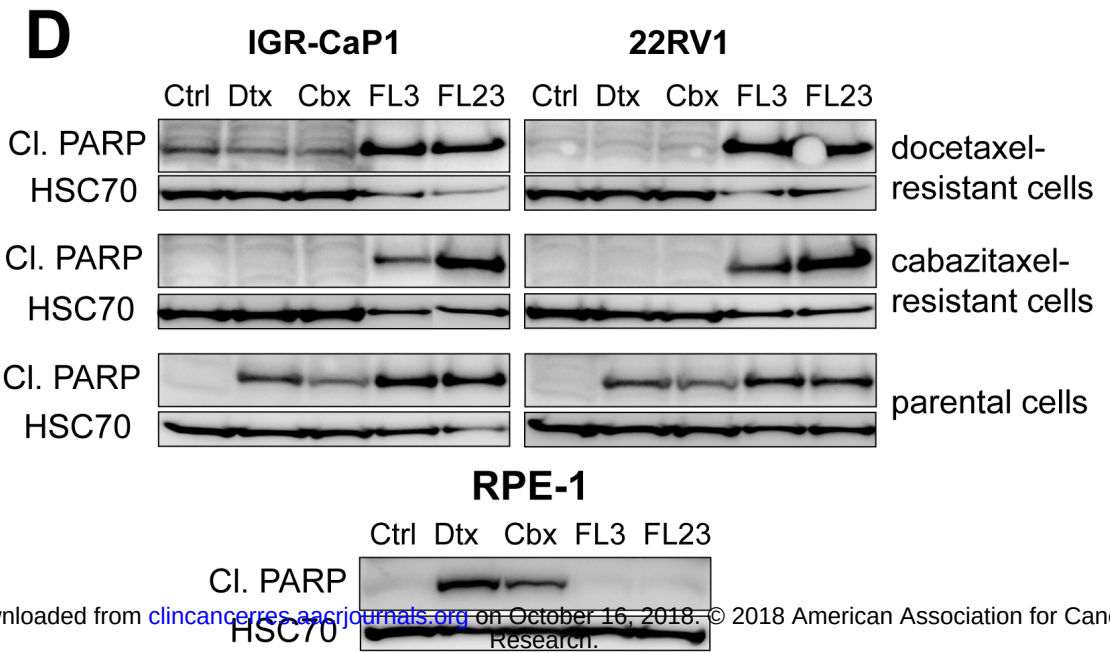

AACR American Association for Cancer Research

Clinical Cancer Research

Regulation of eIF4F translation initiation complex by the peptidyl prolyl isomerase FKBP7 in taxane-resistant prostate cancer

Marine Fanny GARRIDO, Nicolas JP MARTIN, Matthieu BERTRAND, et al.

Clin Cancer Res Published OnlineFirst October 15, 2018.